Journal of Colloid and Interface Science 506 (2017) 620–632

Contents lists available at ScienceDirect

Journal of Colloid and Interface Science

journal homepage: www.elsevier.com/locate/jcis

# Influence of carbon nanoparticle modification on the mechanical and electrical properties of epoxy in small volumes

Christian Leopold [a,*], Till Augustin [a], Thomas Schwebler [a], Jonas Lehmann [a], Wilfried V. Liebig [b], Bodo Fiedler [a]

[a] Hamburg University of Technology, Institute of Polymer Composites, Denickestrasse 15, D-21073 Hamburg, Germany
[b] Karlsruhe Institute of Technology (KIT), Institute of Vehicle System Technology, Rintheimer Querallee 2, D-76131 Karlsruhe, Germany

## GRAPHICAL ABSTRACT

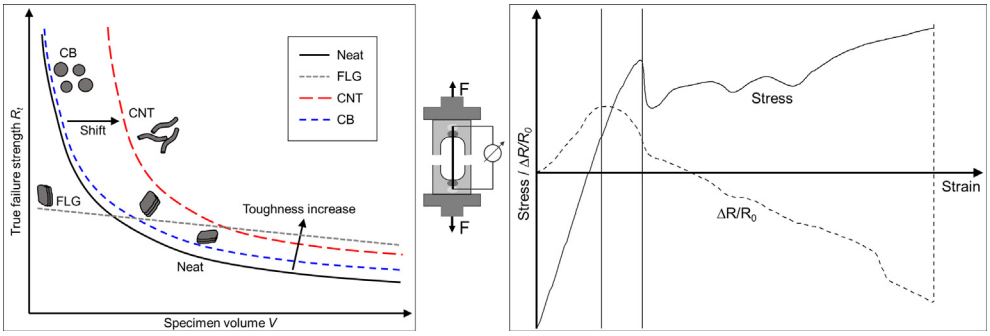


## ARTICLE INFO

*Article history:*
Received 29 March 2017
Revised 4 July 2017
Accepted 22 July 2017
Available online 25 July 2017

*Keywords:*
Sensing
Percolation behaviour
Fractography
Structural health monitoring
True failure strength
Damage mechanisms

## ABSTRACT

The influence of nanoparticle morphology and filler content on the mechanical and electrical properties of carbon nanoparticle modified epoxy is investigated regarding small volumes. Three types of particles, representing spherical, tubular and layered morphologies are used. A clear size effect of increasing true failure strength with decreasing volume is found for neat and carbon black modified epoxy. Carbon nanotube (CNT) modified epoxy exhibits high potential for strength increase, but dispersion and purity are critical. In few layer graphene modified epoxy, particles are larger than statistically distributed defects and initiate cracks, counteracting any size effect. Different toughness increasing mechanisms on the nano- and micro-scale depending on particle morphology are discussed based on scanning electron microscopy images. Electrical percolation thresholds in the small volume fibres are significantly higher compared to bulk volume, with CNT being found to be the most suitable morphology to form electrical conductive paths. Good correlation between electrical resistance change and stress strain behaviour under tensile loads is observed. The results show the possibility to detect internal damage in small volumes by measuring electrical resistance and therefore indicate to the high potential for using CNT modified polymers in fibre reinforced plastics as a multifunctional, self-monitoring material with improved mechanical properties.



* Corresponding author.
*E-mail addresses:* christian.leopold@tuhh.de (C. Leopold), till.augustin@tuhh.de (T. Augustin), thomas.schwebler@tuhh.de (T. Schwebler), jonas.lehmann@tuhh.de (J. Lehmann), wilfried.liebig@kit.edu (W.V. Liebig), fiedler@tuhh.de (B. Fiedler).

http://dx.doi.org/10.1016/j.jcis.2017.07.085
0021-9797/

## 1. Introduction

The increasing use of polymers and fibre reinforced plastics (FRP) in many industries requires detailed knowledge about failure initiation and propagation within composite laminates. But internal damage in the composite or mechanical degradation behaviour under cyclic loads is very difficult to monitor during operation. Often costly and time consuming non-destructive testing (NDT) methods are necessary to evaluate damage in composite laminates. Early stages of damage like matrix cracks control the design in layers transverse to loading direction [1,2] and limit fatigue life of composite laminates. This leads to an oversizing of composite parts and limit the full potential of the material. Complex damage mechanisms and the possibility of sudden failure of FRP structures demand for periodic inspections, which can be time-consuming and costly especially for large parts. Permanent monitoring of the structure during operation, i.e. with a structural health monitoring (SHM) system, has high potential to increase safety and reduce costs.

One promising approach for increasing mechanical properties of composite laminates is a modification of the matrix with carbon nanoparticles. Furthermore, due to the high electrical conductivity of carbon nanoparticles, the modified matrix can be used as a sensor for structural health monitoring, resulting in a multifunctional material with improved mechanical properties. Multifunctional composites, combining very good mechanical properties with health monitoring capability, are beneficial in many applications. For the use of nanoparticles in FRP, size effects of the material should be considered, because volumes between fibres are tiny. In addition, microstructure and stress state in the neat epoxy compared to the same material as a matrix in a composite may be different [3]. Brittle materials like glass [4], carbon [5,6] and epoxy [7–9] exhibit a size effect due to a statistical defect distribution that results in increasing strength with decreasing volume. Towse et al. [7] found a correlation between defect size and failure strain for an epoxy adhesive. Hobbiebrunken et al. [8] identified a size effect for an epoxy matrix system by comparing the strength of dog-bone specimens and matrix fibres of different diameters.

The influence of different types of carbon nanoparticles on the mechanical properties of polymers and FRP is widely investigated by many research groups. Polymer nanocomposites based on spherical carbon nanoparticles such as carbon black (CB) were investigated previously with regard to electrical percolation [10,11] or fracture toughness of nanoparticle modified polymer [11,12] and FRP [13]. Although no significant improvement in tensile strength is observed for a matrix modification with CB, tensile modulus and fracture toughness are significantly improved, achieving similar fracture toughness values as a modification with multi-wall carbon nanotubes (MWCNT) [12].

Since the rediscovery and popularisation of carbon nanotubes (CNT) in the 1990s [14,15], impressive increase in mechanical properties is reported for CNT modified polymers or FRP [12,13,16–20]. Different energy dissipating and thus toughness increasing mechanisms at the CNT are identified. Among these mechanisms are nanotube pull-out, nanoparticle-matrix debonding and nanotube breakage [12,21]. The importance of CNT dispersion, length and aggregate size on the mechanical and electrical properties of polymer nanocomposites was experimentally investigated by Bai and Allaoui [22] who pointed out that in case of a random orientation of nanotubes, high concentrations are not helpful [22].

Increasing interest is set on graphene nanoparticles after the pioneering work of Novoselov, Geim et al. [23,24]. Graphene based, layered particles such as few layer graphene (FLG) and graphite nano-platelets exhibit high potential for improving mechanical properties [16,25–31]. The fracture toughness and hence strength increase is explained with stress relief due to micro-damage at the nanoparticles. Different energy dissipating damage mechanisms at the nano- or micro-scale are proposed. At the particles itself, graphene layer separation, layer shearing and plastic yielding of the matrix that results in plastic voids are reported [9,16,25,32]. Furthermore, crack pinning and bifurcation, crack deflection as well as crack propagation at different heights at the graphene nanoparticles decrease the crack growth rate and therefore increase the fracture toughness [16,25].

An analytical approach regarding the role of length and cross-sectional shape of fillers on strength and toughness of nanocomposites was presented by Greenfeld and Wagner [33]. Liu and Brinson [34] determined the influence of particle orientation by comparing the reinforcing efficiency. They conclude, that nanoplatelets achieve better reinforcement in the case of random orientation, but nanotubes can generate a larger amount of interphase. With their analytical results, they motivate further experimental comparisons of different nanoparticles in the same polymer matrix [34]. Detailed summaries on the toughening mechanisms for differently shaped nano- or microparticles are given by Quaresimin et al. [16] and by Marouf et al. [35].

Previous investigations on the influence of FLG modification with regard to small volumes have shown that there is a clear size effect for neat epoxy matrix, but only a small increase in strength with decreasing volume for FLG modified epoxy, because FLG particles act as crack initiators, counteracting any size effect due to statistical distributed defects. The true failure strength in small volumes is dependent on the size and orientation of the FLG particles [9]. The influence of other nanoparticle morphologies like CB or CNT on the size effect of epoxy however has not yet been investigated.

For multifunctional materials, the requirements for nanoparticles to improve both, mechanical and electrical properties may be opposing. In example, the highest enhancement of fracture toughness is achieved with an exfoliation method and individual CNTs in the matrix [20], but for electrical conductivity, networks with CNTs being in contact with each other are preferable to obtain electrical conductive paths. Regarding the electrical properties of carbon nanoparticle modified polymers, the filler size and morphology is of great importance besides very high electrical conductivity of the filler itself.

Several approaches of SHM for composite structures have already been investigated [36–41]. One promising approach to monitor composite structures that are electrically conductive is the electrical resistance measurement [42]. In contrast to many other SHM methods, no sensors have to be embedded into or applied onto the structure, since the material itself acts as a sensor. In carbon fibre reinforced polymers (CFRP), the electrical conductivity of the carbon fibres can be used for in situ strain and damage monitoring [43–50]. However, in glass fibre reinforced polymers (GFRP) both, the fibres and the matrix are electrically insulating and electrical resistance measurement is not applicable. The same goes for all other FRP laminates with non-conductive fibre materials.

Modification of a polymer matrix with carbon nanoparticles can lead to a conductive network resulting in an electrically conductive composite material with piezoresistive properties. A conductive network forms above a critical nanoparticle content, the percolation threshold, where the conductivity increases several orders of magnitude. The concept of exploiting the piezoresistive properties of carbon nanoparticle modified polymers for strain and damage monitoring by electrical resistance measurement was first introduced by Kupke et al. [48] and Muto et al. [51]. Fieder et al. [52] were the first to suggest using carbon nanotubes to modify the polymer matrix for damage sensing. Later, several investigations

proved the concept of nanoparticle modification and resistance measurement for strain and damage sensing [53–57]. Recently, Meeuw et al. [58] studied the piezoresistive behaviour of different carbon nanofillers on the piezoresistive response of nanoparticle modified epoxy. They investigated bulk (3D) and film (2D) specimens and explained the mechanisms of resistance increase and decrease due to tensile loading. Panozzo et al. [59] presented an analytical model for the prediction of the piezoresistive behaviour, which shows good agreement with experimental data.

Compared to other nanoparticles, CNT offer the advantage, that due to their high aspect ratio very low percolation thresholds can be obtained. Percolation theory [60] assumes homogeneously distributed particles. However, kinetic percolation, i.e. reagglomeration of particles forming a conductive network, can lead to inhomogeneous particle distribution resulting in percolation thresholds well below the statistically calculated values [61,62]. Despite the aspect ratio ($l/d$) of the nanoparticles, the aspect ratio of the tested volume has an influence on the percolation threshold. Nonetheless, the geometrical influence on the percolation threshold is often neglected in experimental investigations. Most theoretic studies on percolation theory in finite systems consider cubic geometries and only few studies with respect to non-cubic, elongated geometries exist. Theoretical calculations show that the percolation threshold increases for increasing elongation of a finite size volume [63,64]. In FRP laminates, small volumes of polymer matrix between the fibres exhibit an elongated shape. Hence, it is of great interest to investigate the electrical properties and in particular the piezoresistive behaviour of nanoparticle modified polymers in small elongated volumes.

This study aims to investigate the influence of nanoparticle morphology and filler content in polymer nanocomposites on the mechanical and electrical properties in small elongated volumes with regard to the size effect. With an experimental approach representing small volumes, as they are present between the fibres in FRP, the most promising particle morphologies for improving mechanical and electrical properties are discussed. Focus of this work is set on three nanoparticle morphologies: CB, CNT, and FLG. The influence on mechanical properties is discussed comparing the different energy dissipating damage mechanisms at the nanoparticles, in dependence of their respective morphology. The approach of using fibres as specimens has the advantage of very small fracture surfaces [9]. Hence, crack initiation and damage mechanisms at the different nanoparticles can be clearly identified, which is very difficult in larger polymer nanocomposite specimens or FRP because of the complex fracture surface [32]. The aim is further to identify the most suitable nanoparticle morphology for sensors for SHM applications with electrically conductive matrix paths of small volume, by determining the percolation thresholds and analyse how the electrical properties change under tensile load.

## 2. Experimental study

### 2.1. Materials and sample preparation

Epoxy matrix fibres are produced as described in [9] using the resin Momentive Epikote RIMR 135 with the hardener Momentive Epikure RIMH 134 (Density $\rho = 1.13$ to $1.17\ g/m^3$). The epoxy equivalent for RIM 135 is 166–185 g/equivalent and the average amine equivalent for RIM 134 is 52 according to the manufacturer. The resin to hardener mixing ratio is 10:3 as recommended for this system (glass transition temperature $T_g = 93\ ^\circ C$). The method of using epoxy fibres is adapted from Hobbiebrunken et al. [8]. The different types of carbon-nanoparticles used to investigate the influence of particle morphology are listed in Table 1. Concerning the morphology of nanoparticle reinforcements, a categorisation after Tang et al. [65] is used. Dimensions are given considering the morphology of the particles: for the single-wall CNT diameter $d$ and length $l$, for FLG width $w$ and thickness $t$ and for CB the BET surface area.

For the nanoparticle modified fibres, nanoparticles and epoxy resin are mixed inside a glove box and dispersed with a three roll mill (EXAKT Advanced Technologies GmbH 120E) that works on the principle of applying high shear rates on the mixture to disperse the nanoparticles homogeneously. Previous studies have proven, that using a three roll mill to disperse carbon nanoparticles in epoxy leads to an excellent dispersion quality without disturbing size and morphology of the particles [18]. The milling process is repeated seven times at constant rotational speed of the rolls of 33 $min^{-1}$, 100 $min^{-1}$ and 300 $min^{-1}$, respectively. The gap widths are adjusted from 120 µm to 5 µm. The amount of nanoparticles added to the resin is varied in order to firstly, investigate the influence of filling degree on the mechanical properties and secondly, determine the electrical percolation threshold for the different particle morphologies in small, elongated volumes. After dispersion, the hardener is added to the neat or modified resin and the mixture is stirred for approximately 10 min and then degassed under vacuum (15 mbar abs) for 15 min. As can be seen in the SEM images, uniform nanoparticle dispersion is obtained for the different morphologies and filling contents.

Fibres are pulled with a needle from the epoxy when it starts to vitrify. Via the pulling speed of the needle, the fibre diameter can be adjusted to a certain point. The fibres are cut and glued at one end on paper sheets based on ASTM D3379 for single fibre tensile tests [66] and then cured in an oven at 20 °C for 24 h and at 80 °C for 15 h, as recommended for this matrix system. Only one side is fixed in order to avoid tension stresses in the fibres because of thermal or chemical shrinkage during curing. With differential scanning calorimetry (DSC) measurements it is assured that the matrix system is completely cured. The second end of the fibre is fixed on the paper after curing. Behind the glue for fixation on the paper, the fibres are electrically contacted with silver conductive paint. The free test length is 25 mm and the electrical resistance measurement length is $l_E = 27$ mm (refer to Fig. 1).

### 2.2. Single fibre tensile test with electrical resistance measurement and microscopy

Fig. 1 shows a scheme of the developed set-up for tensile tests of epoxy fibres including the measurement of the electrical resistance during mechanical testing. The specimens are mounted in a universal testing machine (Zwick Z100) with a 50 N capacity load cell. A digital multimeter (Keithley 2601A) is connected to both ends of the fibre for measuring the DC electrical resistance during the test. For investigating the distribution of the electrical resistance over the length of a single fibre, fibres are cut into two parts and the electrical resistance of both parts is measured. Subsequently, this procedure is repeated with each of the two parts of the fibres. Four-wire resistance measurement is conducted with a constant voltage of 1 V. The chosen voltage value results in low scatter of the measured resistance when compared with lower voltages. Insulation of the wires to the contacts with the fibre on the paper assures that exclusively the resistance of the fibre is measured and avoids any close circuit via the testing machine.

The side bars of the paper, connecting the upper and lower part of the specimen, are cut before testing. Test speed is set to 25 mm/min in order to minimise plasticity effects with necking and assure a more brittle failure mode of the fibres. The cross section after failure is analysed for each specimen by using an optical microscope (Olympus BX51) and by scanning electron microscopy (SEM) to determine the damage mechanisms at the different types

**Table 1**
Types of carbon nanoparticles used in this investigation (values from the respective data sheets).

| Category | Type | Name | Supplier | Dimensions |
|---|---|---|---|---|
| 0D | CB | Printex 300 | Evonik industries, Germany | BET surface area = 80 $m^2/g$ |
| 1D | CNT | Tuball (75%) | OCSiAl, Russia | $l \geqslant 5$ μm<br>$d \leqslant 1.9$ nm |
| 2D | FLG | AvanGraphene-2 | Avanzare, Spain | 5 μm $\leqslant w \leqslant$ 25 μm<br>$t \leqslant 2$ nm<br>$n_l \leqslant 6$ layers |

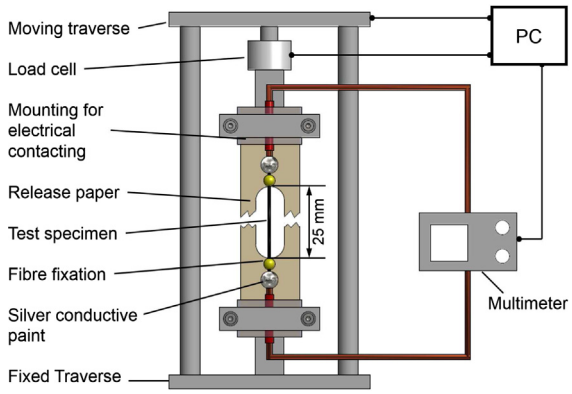


**Fig. 1.** Schematic representation of the test set-up for single epoxy fibres in the universal testing machine with measurement of electrical resistance during the tensile test.

of nanoparticles and the influence of particle size, filling degree and morphology on failure initiation and propagation. SEM is carried out using a Zeiss Leo Gemini 1530 electron microscope by using the SE2 detector with a working distance between 5 mm and 7 mm at 1 keV and without sputtering of the surface. For some CNT modified specimens, a mixture of the SE2 detector with the inLens detector at an acceleration voltage of up to 8 keV is used. The true failure strength $R_t$ is determined from the measured force at failure and the cross section area obtained by microscopy. The fracture of the fibres is regarded as brittle.

## 3. Results

### 3.1. Mechanical properties

Fibre tensile test results are presented in Fig. 2 with regard to the influence of specimen volume as well as nanoparticle morphology and filling content on true failure strength. Open symbols for neat and FLG modified fibres are values from previous work [9] and are given for comparison. Fig. 2(a) shows the true failure strength $R_t$ for neat and with 0.05 wt.% carbon nanoparticles modified epoxy fibres as a function of specimen volume. Strength values exhibit a size effect for neat epoxy and a limitation in true failure strength at approximately 110 MPa for fibres modified with 0.05 wt.% FLG. The CB modified epoxy exhibits a clear size effect, comparable to the neat material. For small volumes, an increase in true failure strength of approximately 100 MPa is observed. In comparison to the neat epoxy fibres, the CNT modified fibres exhibit slightly higher true failure strength at similar volume. One CNT fibre with volume of $V = 0.91$ $mm^3$ exhibits high true failure strength of $R_t = 154.7$ MPa for the comparable high volume. The fracture surface of this fibre is further examined in fractography to identify possible reasons for this behaviour (refer to Fig. 5). For a CNT content of 0.05 wt.%, no significant size effect is visible, but for lower particle content, increasing strength with decreasing volume and therefore a clear size effect is observed (refer to Fig. 2 (c)).

The influence of nanoparticle volume fraction with regard to true failure strength is shown in Fig. 2(b) for CB, in Fig. 2(c) for CNT and in Fig. 2(d) for FLG modified fibres, respectively. For CB modified epoxy, configurations with 0.05 wt.% and 0.5 wt.% nanoparticle content are regarded. No influence of nanoparticle weight content in this range on true failure strength of the specimens is observed. Although the number of tested specimens for this configuration is comparably small, especially for 0.5 wt.% ($n = 3$), the highest value of all specimens for true failure strength of $R_t = 226$ MPa is measured at a volume of $V = 0.06$ $mm^3$. The lowest value for true failure strength $R_t$ of this configuration is measured for a specimen with the same volume, which is comparable to the values of neat epoxy fibres. The neat specimens also exhibit large scatter at low volumes due to the statistical distribution of defects owing to the fact, that only the largest defect initiates final failure. The similar behaviour of neat epoxy and CB modified epoxy can be explained with a failure initiation at surface defects that is observed in SEM images for both types. A larger defect results in lower true failure strength.

Three configurations of CNT modified epoxy are tested: 0.025 wt.%, 0.05 wt.% and 0.5 wt.%. For CNT modified epoxy, values of true failure strength in the range of 200 MPa are observed just for the lowest filling content of 0.025 wt.% CNT. This indicates, that with lower filling content a size effect for CNT modified epoxy exists as well. But failure initiation has to be analysed more in detail and will be done by fractography analysis of the fracture surfaces as described in Section 3.2. It should be highlighted, that the highest $R_t$ values 190 MPa and 206 MPa for CNT modified epoxy are in the range of the maximum values for the neat epoxy, but for specimens with significantly higher volume. This implies that despite the size effect, the CNT modification has a positive effect on failure stress.

For FLG modified epoxy, no significant influence of the amount of nanoparticles in the matrix is found. This is attributed to failure initiation at the largest FLG particle or aggregate, which is larger than any material defects, thus always available within the fibre and independent of specimen volume [9]. Most values for true failure strength are between 60 MPa and 110 MPa. For higher FLG filler content, $R_t$ values rise up to 130 MPa for 0.1 wt.% FLG and 140 MPa for 0.5 wt.% FLG. Hence, only a small increase in $R_t$ but no significant size effect when compared to neat or CB modified epoxy is observed. The true failure strength of FLG modified epoxy depends on two factors: 1. the size of the largest FLG particle that initiates failure, 2. the orientation of this particle with regard to loading direction [9]. This will be analysed more in detail by SEM of the fracture surfaces (refer to Section 3.2) and discussed in Section 4.1.

### 3.2. Fractography

The fracture surfaces of the fibres after tensile testing are analysed by SEM with regard to failure initiation and damage mecha-

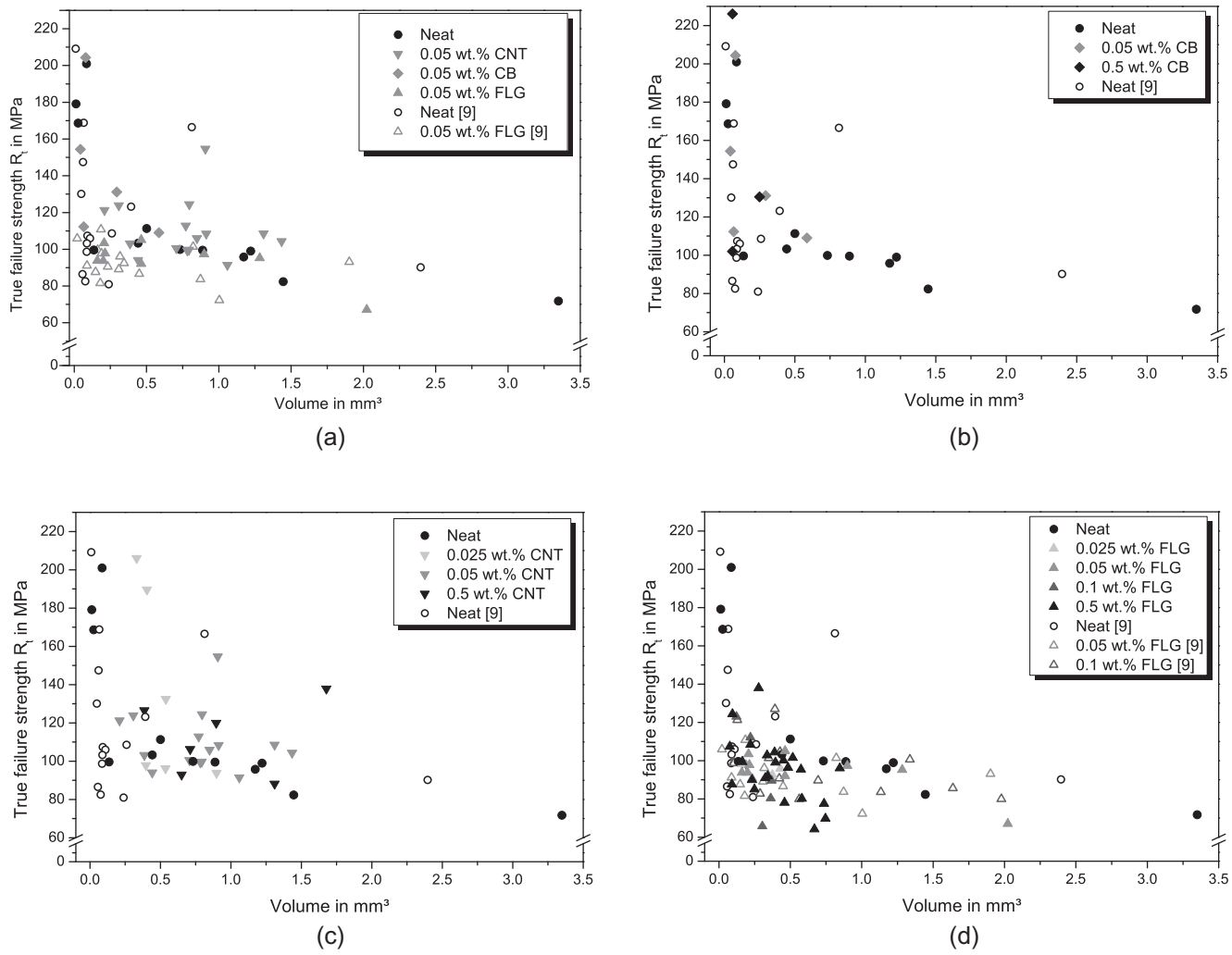


**Fig. 2.** True failure strength versus specimen volume for neat and with carbon nanoparticles modified epoxy fibres showing the influence of nanoparticle morphology at 0.05 wt.% particle concentration (a) and of nanoparticle filling content for (b) CB (c) CNT and (d) FLG modified epoxy (values with open symbols out of [9]).

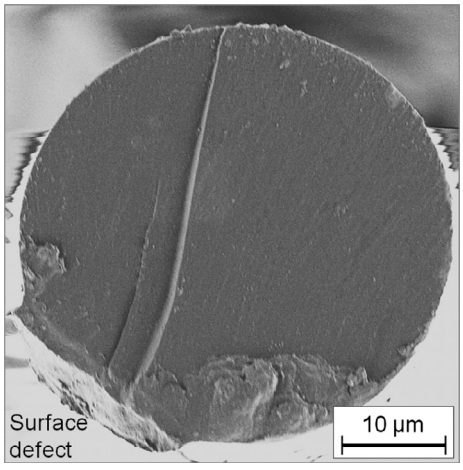


**Fig. 3.** SEM image of a representative fracture surface of a neat epoxy fibre showing failure initiation at a surface defect.

nisms at the nanoparticles. Fracture surfaces of neat epoxy fibres are smooth. An example of a representative fracture surface is given in Fig. 3. Failure initiates at surface defects and the defect size can be correlated with the true failure strength. A representative fracture surface of a with 0.5 wt.% CB modified epoxy fibre is shown in Fig. 4. Failure initiates at a surface defect that is larger than the nanoparticles or small CB agglomerates visible in the fracture surface. The fracture surface is rougher compared to that of neat epoxy, which indicates a potential for fracture toughness increase. Crack separation and crack propagation at different heights are visible and may act as energy dissipating damage mechanisms at the globular shaped CB nanoparticles.

Fig. 5 shows representative fracture surfaces of CNT modified epoxy fibres. Failure initiates either at CNT agglomerates (refer to Fig. 5(a) and (b)) or at inclusions like amorphous carbon or other foreign particles (refer to Fig. 5(c)). These inclusions act like defects in the material and initiate failure due to local stress concentrations. An inclusion is shown in detail in Fig. 5(d). Energy dispersive X-ray (EDX) analysis performed in SEM reveals a high concentration of iron. We assume these inclusions to be remnants from the ferrocene catalyst used in the CNT production process, because we observed them only in CNT modified fibres. The higher the CNT filler content, the higher the probability of such impurities being present in the fibre. If no inclusions are present, failure initiates at the largest CNT agglomerate in the fracture surface. Such a CNT agglomerate is shown in Fig. 5(b). An increase in CNT weight fraction in the matrix increases the fracture surface roughness and thus indicates higher toughness [20,67]. Crack separation at CNT

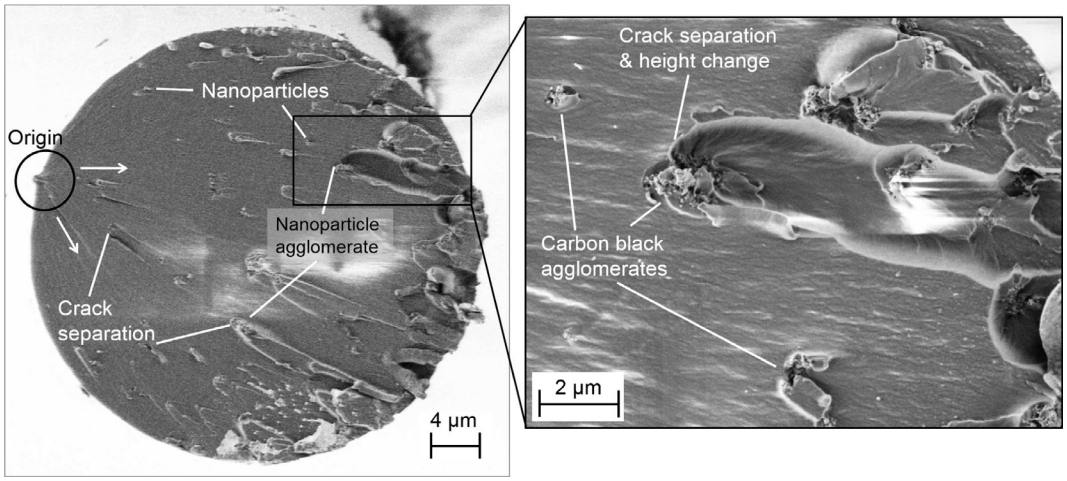


**Fig. 4.** SEM image of a representative fracture surface of a with 0.5 wt.% CB modified epoxy fibre (V = 0.06 mm$^3$, $R^t$ = 226.11 MPa), showing crack separation at CB particles and agglomerates.

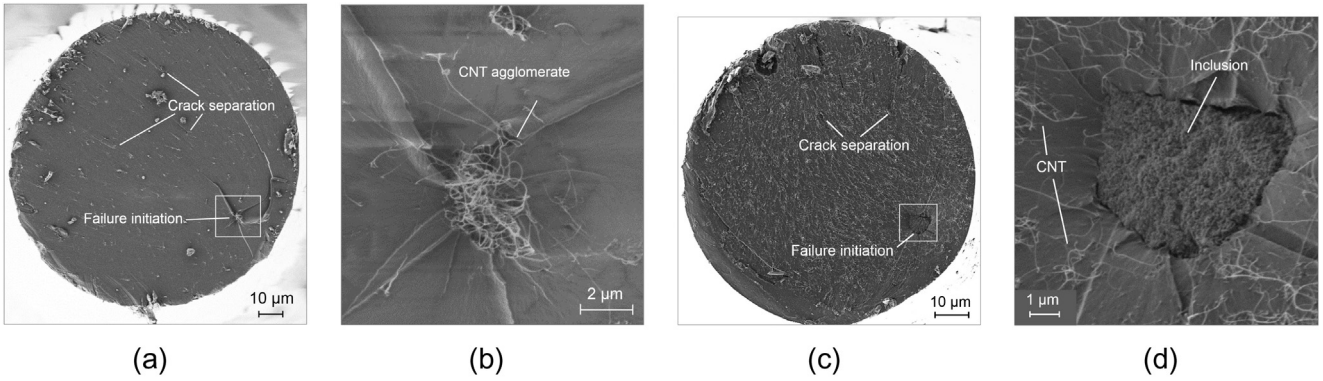


**Fig. 5.** SEM images of representative fracture surfaces of epoxy fibres modified with carbon nanotubes: (a) fibre modified with 0.05 wt.% CNT ($V = 0.91$ mm$^3$, $R_t = 154.69$ MPa), showing crack initiation at a CNT agglomerate and crack separation at CNT particles, (b) detail of the CNT agglomerate in (a), (c) fibre modified with 0.5 wt.% CNT ($V = 0.39$ mm$^3$, $R_t = 126.57$ MPa), showing crack initiation at a non-carbon inclusion, (d) detail of failure initiating inclusion in (c).

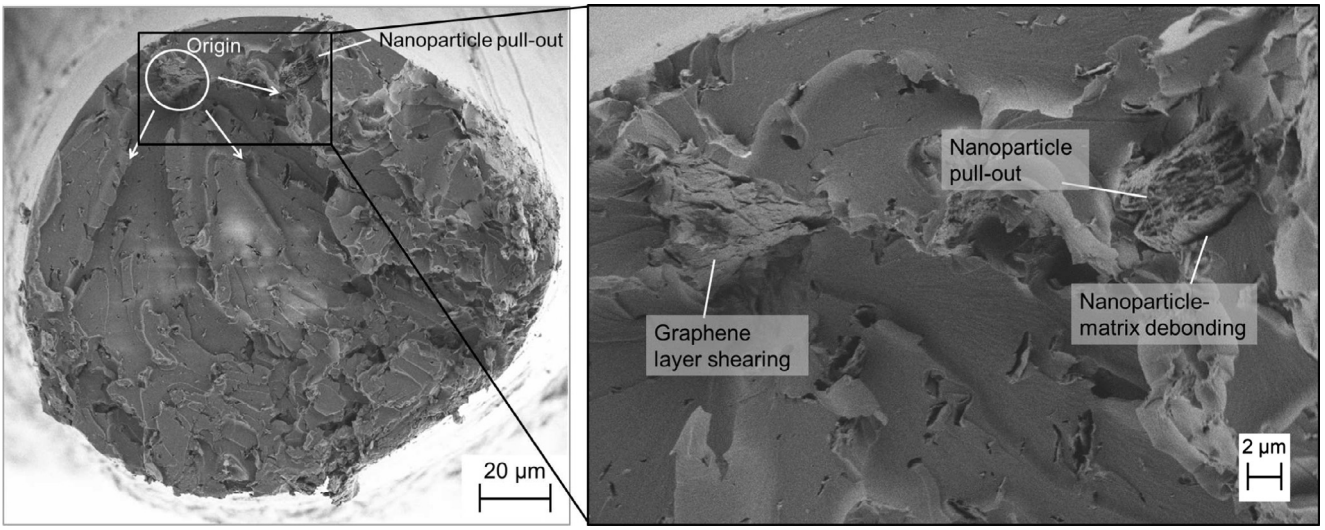


**Fig. 6.** SEM image of a representative fracture surface of an epoxy fibre modified with 0.05 wt.% FLG ($V = 0.58$ mm$^3$, $R_t = 80.19$ MPa), showing crack initiation at an FLG particle, FLG pull-out failure mechanisms at another particle and a very rough fracture surface.

aggregates is visible. Nanotubes that are pulled out of the fracture surface are visible, the amount being significantly higher for 0.5 wt.% CNT compared to 0.05 wt.% CNT content. Pulled-out tubes are partly oriented in crack growth direction. This is shown more detailed in Fig. 9.

Fig. 6 shows an SEM image of a representative fracture surface of a fibre containing 0.5 wt.% of FLG particles. Similar to the CNT modification, an increase in nanoparticle content leads to a rougher fracture surface. The damage mechanisms of nanoparticle pull-out, plastic void growth at the particles and graphene layer shearing at the FLG particles, already discussed in [9,16,25,32], are observed. Increasing nanofiller content increases the amount of matrix plastic deformation and hence the fracture surface roughness. Failure initiates at the largest FLG aggregate in the fracture surface. In Fig. 6, two FLG aggregates of similar size are visible. The graphene layers in the failure initiating particle are oriented nearly perpendicular to loading direction, whereas the layers in the other FLG particle are oriented parallel to loading direction. This confirms that despite the size of the particle, the orientation with regard to loading direction is critical [9]. The large amount of FLG modified fibres allows to quantify the influence of particle or aggregate orientation on the true failure strength. Assuming that failure always initiates at the largest FLG particle or aggregate in the volume, fracture surfaces of several FLG modified specimens regarding the orientation of the failure initiating FLG particle are analysed. The orientation of this particle related to loading direction is correlated with the volume and true failure strength of the respective specimen, as shown in Fig. 7. True failure strength of the particles oriented perpendicular or diagonal to loading direction is limited to approximately $R_t = 105$ MPa. The layers oriented perpendicular to loading direction may separate at lower stresses due to the comparable weak Van-der-Waals forces between the layers and initiate failure. When the FLG particles are oriented with the layers in loading direction, the modified fibres exhibit true failure strength above $R_t = 105$ MPa and up to $R_t = 140$ MPa. FLG particles oriented perpendicular to loading direction are observed only in fibres of larger volume. This can be explained by the fibre/FLG particle diameter ratio. If the fibre diameter approaches the lateral FLG dimensions, which may be up to 20 µm, the fibre is prone to break during the manufacturing process. Therefore, in the smaller fibres produced, the largest FLG particles are oriented almost in loading direction. With smaller volume, the probability of the comparable large FLG particles to be oriented transverse to loading direction decreases, leading to higher failure stress. This leads to the observed occurrence of parallel to loading direction oriented particles only in fibres with smaller volume.

### 3.3. Electrical properties

In this section, the electrical characterisation results are shown, including percolation threshold and the resistance distribution over the length of a single fibre. Subsequently, the resistance change during tensile loading is presented.

#### 3.3.1. Percolation threshold and resistance distribution

For CB and FLG modified epoxy fibres, the electrical conductivity is below the measuring limit. Therefore, the percolation thresholds of these fibres are above the value of the highest investigated nanoparticle concentrations of 15.0 wt.% and 2.4 wt.% for CB and FLG, respectively. The electrical resistance of CNT modified fibres is measurable and fibres with different nanoparticle concentrations are characterised. Electrical conductivities over CNT particle concentrations for the tested fibres are plotted in Fig. 8. The fibres with CNT contents below 0.3 wt.% exhibit a conductivity below the measuring limit (except for two specimens). A percolation threshold of 0.3 wt.% CNT is determined from the two different conductivity levels and the significant increase of conductivity at this CNT concentration.

SEM images of fracture surfaces, as shown exemplarily in Fig. 9, highlight the structure of the CNT network. A dense network formed by homogeneously dispersed nanoparticles is visible for fibres with a CNT content of 0.5 wt.%. For fibres with CNT contents below the percolation threshold no conducting networks are visible (see Fig. 5). As discussed in Section 3.2, the visible orientation of the CNT is attributed to pulled-out particles lying in crack growth direction. For the investigations presented in the following a CNT content above the percolation threshold of 0.5 wt.% is chosen to achieve electrical conductivity and piezoresistive behaviour of the fibres.

Fig. 10 shows the resistance measured at adjacent parts of one exemplary fibre. The solid horizontal line indicates the measured resistance per length of the whole fibre and the dashed horizontal

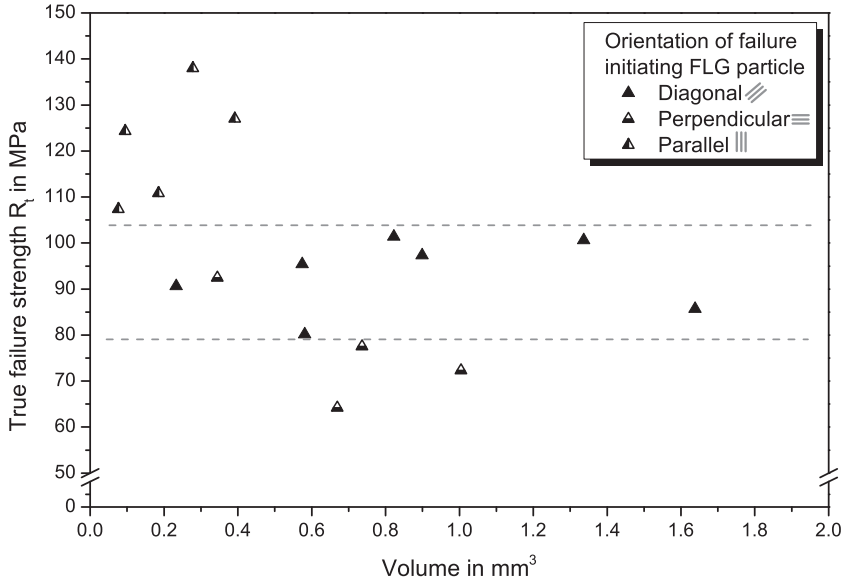


**Fig. 7.** Influence of FLG-particle orientation with regard to loading direction on true failure strength for different volumes.

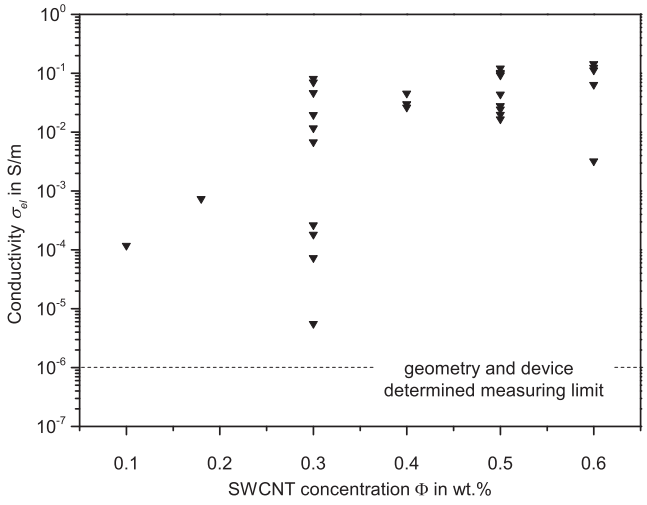


**Fig. 8.** Percolation curve of SWCNT modified epoxy fibres.

lines represent the resistance per length $l_e$ of the halves of the fibre cut into two parts. Grey columns display the resistance per length of the quarter parts of the fibre cut into four parts. A difference in the resistance per length of the two parts as well as of the four parts can be observed. This indicates a non-homogeneous distribution of the resistance over the length of the fibre. Fig. 11 shows the ratio of measured resistance $R$ to resistance of the uncut fibre $R_1$ versus the ratio of fibre length $l_e$ to the length of the uncut fibre $l_{e1}$. Three representative fibres with different diameters are shown. Measured values of fibre halves are plotted on the right side ($l_e/l_{e1} > 30\%$), whereas the left side ($l_e/l_{e1} < 30\%$) shows the values measured for the quarters of the same fibres. Theoretically, assuming homogeneous resistance distribution over the fibre length $R/R_1 = l_e/l_{e1}$ applies. This relation is indicated by the dashed line. As can be seen in Fig. 11 this theoretical relation is not exactly applicable in practice due to scattering of the measured values. The scatter indicates that the resistance is not distributed homogeneously over the fibre length. For example the shortest part of fibre 2 (indicated by circles) has a higher resistance, compared with the three other sections of the same fibre in the region of $l_e/l_{e1} = 12-15\%$. Furthermore, smaller fibres tend to show a higher scatter in resistance over the length.

*3.3.2. Electrical resistance measurements during tensile tests*

Fig. 12 shows a representative stress-strain curve of a fibre with a CNT content of 0.5 wt.% during tensile testing with synchronous electrical resistance measurement. The stress and the resistance change are shown as continuous and dashed lines, respectively. The stress is calculated from the original fibre cross section and the strain is calculated using displacement data from the moving traverse of the universal testing machine and the original fibre length. Due to the small specimen size no other strain measurement is applicable. The stress-strain curve shows a linear region (up to $\varepsilon = 2.1\%$ strain) followed by plastic deformation and yielding (at $\varepsilon = 3.4\%$ strain). Then multiple necking occurs until final fracture at $\varepsilon = 13\%$ strain. The resistance increases exponentially, followed by a point of inflexion and reaches a maximum at $\varepsilon = 2.1\%$ strain. The resistance decreases continuously for increasing strain and drops below the initial resistance for high strains.

## 4. Discussion

### *4.1. Mechanical properties*

Particle morphology has a clear influence on the size effect and the maximum true failure strength of modified epoxy. If nanoparticles or nanoparticle aggregates are larger than the statistically distributed defects always existent within the material, they initiate failure and thus neglect any size effect. This is the case for the comparable large FLG particles used in the present study. Otherwise, if nanoparticles are smaller than material defects, a size effect with increasing strength for decreasing volume exists. This is the case for CB particles or even small CB agglomerates and may be beneficial in small volumes, i.e. between the fibres of FRP. According to the experimental results, a size effect is also observable for CNT modified epoxy if purity and dispersion are of high quality.

The SEM images show, that dispersion of CNT with the calendering method is very efficient even for CNT with a very high specific surface area (small diameter, high length). They are an optimum for mechanical and electrical properties, but difficult to disperse homogeneously in the matrix [12,18]. Good dispersion is achieved for CB and FLG as well, confirming the three-roll-mill dispersion method as highly efficient for different particle morphologies [18,68]. Although SWCNT have a high potential for increasing tensile strength [12], the presence of undesired remnants from the production process may counteract any enhancement, as is the case in several fibres in this study. Accordingly, in order to achieve an optimum in reinforcement, dispersion and purity of the

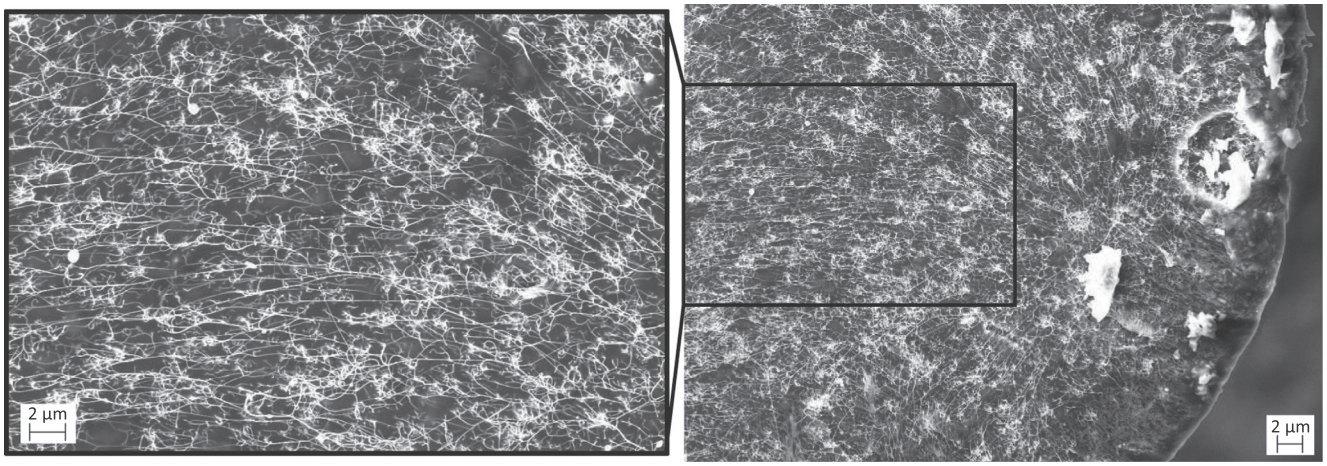


**Fig. 9.** SEM image of representative fracture surface of an epoxy fibre modified with 0.5 wt.% CNT resulting in an electrically conductive nanoparticle network. Epoxy and CNT are displayed in dark grey and white, respectively.

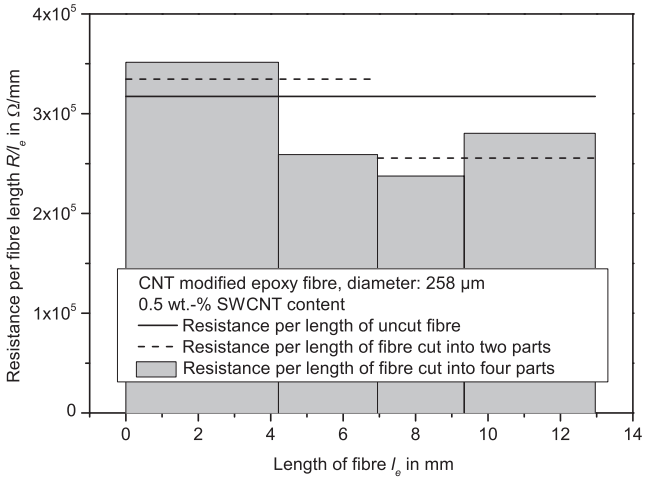


**Fig. 10.** Resistance measured on cut fibre parts over the length of the fibre.

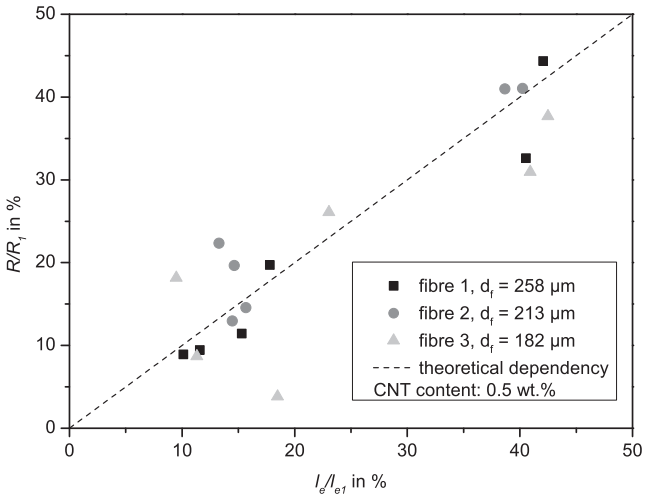


**Fig. 11.** Ratio of fibre section resistance to resistance of uncut fibre versus ratio of fibre section length to length of uncut fibre.

nanoparticles are critical and should be considered carefully. Impurities from nanotube production act as flaws within the material and oppose the desired enhancement. The observed failure initiation at CNT agglomerates is in accordance with other experimental results, i.e. from Bai and Allaoui [22].

The high values of true failure strength at smaller volumes for CB modified epoxy exhibit a certain potential for increasing mechanical properties of polymers and FRP with these comparable cheap fillers. This is due to the fracture toughness increase, reported in [12]. The toughening mechanism of crack separation and plastic yielding of the matrix at the CB particles is shown in Fig. 13 schematically and in the SEM image of a fracture surface. This is comparable to the mechanism shown by Haba et al. [68] for fullerene like tungsten disulfide ($WS_2$) particles that have similar morphology. Because of the globular shape of CB, additional energy dissipating mechanisms, like pull-out or layer shearing are not available for this type of particles. Compared to the other particles, the zone around a particle available for energy dissipation is very small, confirming our assumption of a point-like 0D enhancement.

The highest true failure strength values of neat and CNT modified epoxy are in the same range, but those of the latter are measured in specimens of larger volume. The CNT modification therefore increases the tensile failure strength of polymers. What is reported in literature for bulk specimens [12,18–20] is now confirmed for very small, elongated volumes. As energy dissipating, toughening mechanisms at the nanoscale, nanotube fracture, crack bridging and nanotube pull-out are identified, with the latter being most pronounced in the fracture surfaces. A scheme (adapted from [12]) and SEM images showing the dominant mechanisms in the fracture surface are given in Fig. 14. Since nanotube pull-out is the dominating mechanisms at nanoscale and it can only be effective in dissipating energy along the nanotube direction, the categorisation of CNT as 1D reinforcement seems to be valid. The size effect - a significant increase in strength below a certain volume – is valid for CNT modified polymer as well, but the volume, at which strength increases significantly, is shifted to higher values.

Concurring effects are present for FLG modification. For most effective improvement of mechanical properties, a particle size close to the critical length is desired [33], but larger particles or aggregates may initiate failure in small volumes at lower stress, compared to the unmodified material. Hence, larger particles

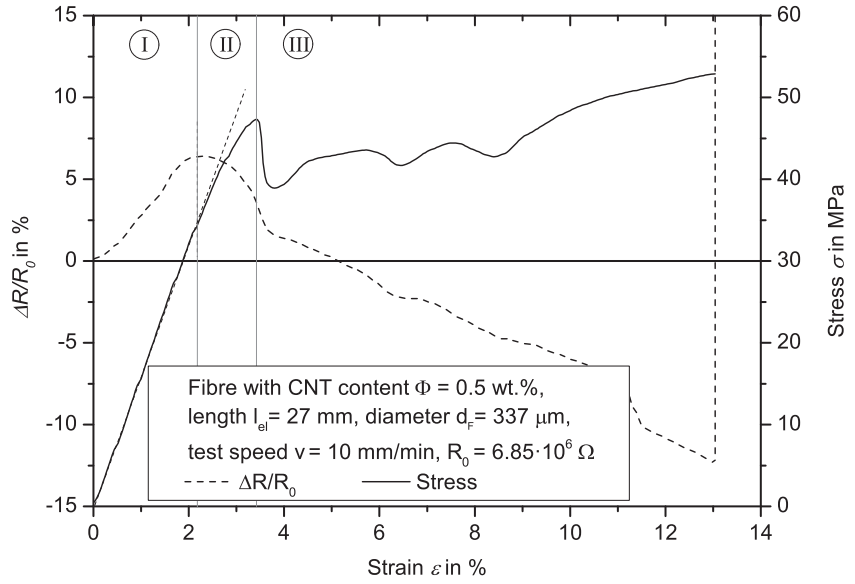


**Fig. 12.** Stress-strain curve and electrical resistance change of a single matrix fibre modified with 0.5 wt.% CNT in fibre tensile test.

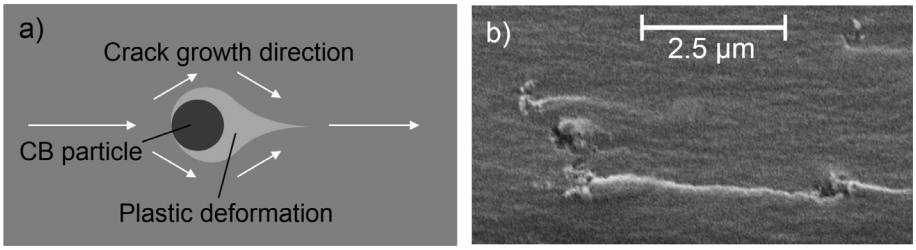


**Fig. 13.** Damage mechanisms at carbon black particles: (a) Scheme for crack separation at a CB nanoparticle or agglomerate (b) SEM image showing local matrix plastic deformation and crack separation at CB particles in a matrix fibre fracture surface.

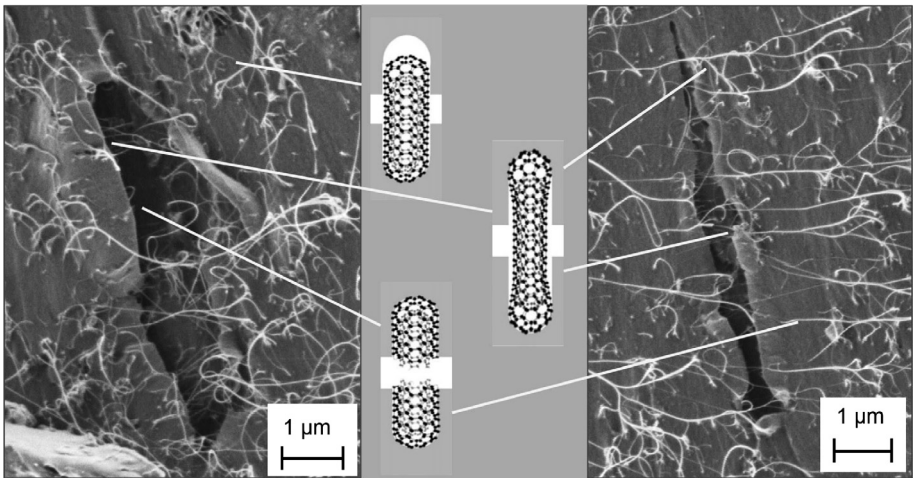


**Fig. 14.** Different damage mechanisms at carbon nanotubes: schematic representation of the nano-damage mechanisms crack bridging, nanotube pull-out and nanotube fracture after [12] and SEM images of these mechanisms in the fracture surface of a matrix fibre modified with 0.5 wt.% CNT.

may have negative effects on some mechanical properties. For FLG modified epoxy, a clear influence of the particle orientation with regard to loading direction is quantified (shown in Fig. 7). Failure initiates at the largest FLG particle or aggregate. Orientation of the covalent bonds within the graphene layers of this particle in loading direction leads to damage initiation at higher stresses and thus, higher true failure strength. In small elongated volumes like in the spaces between the fibres in FRP, a perpendicular orientation of the graphene layers is not possible, if lateral dimensions of the FLG particles are in the range of the fibre diameter. For diagonal or perpendicular orientation of the largest FLG particle, true failure strength of the specimens is limited to 105 MPa. This is the maximum global stress value at which local layer shearing, layer separation or plastic yielding of the matrix occurs and initiates final failure. The damage mechanisms of FLG pull-out occurs at latest at a maximum stress of 140 MPa. Due to the high stiffness difference between fibre and matrix, local stress concentrations occur. Considering this, calculations of the maximum failure strength of either the Van-der Waals bonds between the layers or the nanoparticle-matrix interface can be verified by using these experimental results. The results also implicate that in FRP, the particles are oriented along the reinforcing fibres. In 0°-layers, the covalent bonds of the FLG particles are oriented in loading direction. In 90°-layers, the layers are oriented perpendicular to loading direction and may on one hand initiate local failure but on the other hand dissipate energy due to the shearing of the graphene layers and plastic deformation of the surrounding matrix, leading to enhanced mechanical properties observed when incorporated in FRP [65,32].

As expected, the fracture surface roughness increases with increasing filler content for all configurations. Comparing the plastic deformation of the matrix for the three nanoparticle types, FLG modification exhibits the highest amount of fracture surface deformation, whereas in CB modified specimens only rough spots at agglomerates are found, where the crack height is changed. CNT modification in general leads to higher amounts of plastic deformation compared to CB, but pull-out of the nanotubes is the dominant mechanism. The nanotubes used in this study are quite long and pull-out length is high before breakage. According to analytical approaches [33], this should result in a significant increase in strength and toughness and explains both, the higher stress values compared to the neat fibres of same volume and the shift of the strength increase, due to the size effect, to higher volumes.

The nanoparticle volume fraction may have a significant influence on mechanical properties of nanocomposites [12,18,25]. Regarding the size effect, no significant influence of a modification with FLG or CB nanoparticles is found. In FLG modified epoxy, a failure initiating particle is always available, neglecting any size effect, whereas for CB, the particles are smaller than material surface defects, resulting in a similar behaviour as the neat epoxy. With decreasing filling content, CNT modified epoxy exhibits less probability of agglomerates or impurities from manufacturing process, resulting in a more significant size effect. Nonetheless, if purity and dispersion are high enough, it is assumed that the CNT weight fraction has no significant influence on the size effect up to a certain volume fraction.

Concluding, the influence of the investigated particle morphologies on the size effect according to the experimental results is presented schematically in Fig. 15. As there is a clear dependence on particle size, epoxy modified with smaller graphene particles may also exhibit a size effect.

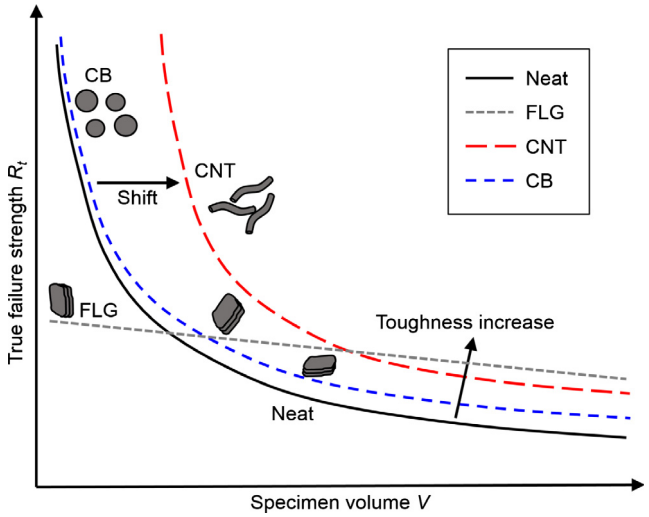


**Fig. 15.** Influence of carbon nanoparticle morphology on the size effect of epoxy matrix nanocomposites.

### 4.2. Electrical properties

The percolation thresholds of $\Phi > 15$ wt.% for CB, $\Phi > 2.4$ wt.% for FLG, and $\Phi = 0.3$ wt.% for CNT lie above typical percolation thresholds reported in literature [58,62,69]. This can be explained by two mechanisms. Firstly, the nanoparticles are well dispersed and homogeneously distributed and the level of kinetic percolation is very low. Secondly, the fibrous geometry with its high aspect ratio statistically results in higher percolation thresholds, since the probability of conductive paths decreases for increasing length to diameter ratio.

For small volumes, for instance in the interspaces of fibres in FRP, this effect is often neglected but needs to be considered for choosing an appropriate nanoparticle content resulting in the desired piezoresistive properties. The resistance is not distributed homogeneously over the length of the fibres. The reason for this is a statistical distribution of the particles and the linked amount of redundant conductive network paths, which varies over the fibre length. For decreasing cross sections this influence increases due to a decreasing redundancy of network paths at the same nanoparticle content. Furthermore, variations of the fibre diameter can cause varying conductivity over the length of the fibre. Both effects explain the trend of increasing scatter with decreasing fibre diameter. The stress-strain curve is divided into three characteristic regions (see Fig. 12) and the piezoresistive behaviour is explained according to these regions.

- **Region I**: The fibres exhibit linear elastic followed by linear viscoelastic stress-strain behaviour. The resistance change shows an exponential increase followed by a point of inflexion and a maximum of $\Delta R/R_0 = 5\% \pm 1\%$ for all tested specimens. Since the Poisson's ratio of the matrix ($\nu = 0.38$) is smaller than 0.5, the tensile loading increases the specimen volume and therefore the average distance of the CNT increases as well. This increase of particle distance leads to an exponential increase of the tunnelling resistance, which mainly determines the electrical resistance of CNT modified polymers [70]. Hence, the resistance of the specimen increases exponentially as well. In contrast to the increase of the particle distance in length direction, the particle distance in width direction decreases, leading to a resistance decrease.
- **Region II**: Non-linear viscoelastic and irreversible deformation occur and the matrix starts to yield. The transverse contraction increases further, causing a particle distance decrease in transverse direction and therefore the tunnelling resistance decreases. Due to stress peaks induced by the particles, local viscoelastic and plastic deformation and local plastic yielding occur, leading to thinner epoxy layers between the particles and thus to a smaller distance and decreasing tunnelling resistance. Shui and Chung [71] and Meeuw et al. [58] reported similar behaviour for 3-D and 2-D volumes. At the resistance maximum, the opposing effects that influence the tunnelling resistance compensate. On the one hand, the particle distance increases due to strain in fibre direction, on the other hand, it decreases due to transverse contraction and thinner epoxy layers between the particles due to plastic yielding. These opposed effects have a comparable influence on the tunnelling and thus on the measured resistance. Hence, at this point both effects level out and no resistance change is observed.
- **Region III**: At yield stress, necking of the fibres occurs and the effects of transverse contraction and yielding of the matrix dominate, resulting in local thinner epoxy layers between the nanoparticles. The tunnelling gaps and with them the measured resistance decrease. Multiple necking occurs and the electrical resistance decreases in all these necked regions, resulting in a continuous resistance decrease until final fracture of the specimen, which leads to an unmeasurable high resistance. Final failure separates the electrical conductive path by rupture of the specimen, which results in a non-measurable high resistance.

With the described characteristic of the resistance change due to tensile loading, CNT/polymer composites with small elongated volumes can be used as strain sensors. The resistance maximum is located at the beginning of local plastic deformation of the matrix, indicated by a decrease in the slope of the stress-strain curve (refer to Fig. 12, slope change indicated by a dotted line). Thus, CNT modified epoxy can be used as a sensor to detect the initiation of plastic deformation and with it the initiation of irreversible damage of the material at the maximum of the measured resistance. For most applications, the ambiguity of the resistance signal, which occurs at higher strains is not problematic, because due to the stiffer fibre reinforcement, fracture in FRP occurs at lower strains than those at which the resistance decreases (see also [58]).

## 5. Conclusion

With a carbon nanoparticle modification, multifunctional materials combining electrical conductivity for damage sensing with enhanced mechanical properties are obtained. Particle size and morphology are key factors in this context when regarding small volumes, because larger particles may initiate failure prior to material defects. With a new concept of simultaneous testing of mechanical and electrical properties in small elongated volumes, a clear size effect, similar to the unmodified material can be measured for CB and CNT modified epoxy, whereas for FLG, the used particle size is larger than material defects and thus failure initiates at the particles. Also for electrical properties a size effect is found to exist. Carbon nanoparticle modified epoxy exhibits a significantly higher percolation threshold in small elongated volumes compared to the bulk material. For applications such as electrically conductive nanoparticle modified polymer wires, a larger amount of particles is necessary to use these volumes for sensing applications.

Different nanoparticle morphologies show different failure mechanisms at the nano- or micro-scale. For CB modification, crack separation and local matrix plastic deformation are reported. The dominant mechanism in CNT modified specimens is pull-out of nanoparticles, but crack bridging and nanotube rupture are also

observed. For FLG modified epoxy, energy dissipating damage mechanisms are matrix shear yielding leading to plastic voids, graphene layer separation and shearing as well as pull-out of particles. The mechanisms can be clearly identified in the small fracture surfaces. For FLG, the orientation of the graphene layers with regard to loading direction is critical. Higher true failure strength is measured with the largest particle oriented parallel to loading direction. From a mechanical properties point of view, FLG and CNT are the most promising particle morphologies, if CNT length is high enough and FLG are oriented in loading direction. CNT modified fibres are well suited as electrical conductive paths since the amount of filler can be adjusted in a way that the beginning of plastic yielding is identified by the maximum of resistance change. Furthermore, until onset of plastic yielding the resistance change can be used as a strain sensor. CB and FLG are identified to be not suitable to form a conductive network in small elongated volumes since percolation thresholds are very high.

To conclude, for multifunctional polymer or FRP materials, CNT with a weight fraction above 0.3 wt.% are shown to be the most promising nanoparticle filler for improving both, electrical and mechanical properties, even in small elongated volumes. With this modification, smart structures for health monitoring with improved mechanical properties can be designed. Further research should focus on the applicability of the proposed SHM method using electrical conductive paths in FRP laminates and structures.

## Acknowledgement

This work was carried out with funding from the German Research Foundation (DFG) within the project number FI 688/5-1. This financial support is gratefully acknowledged. The second author kindly acknowledges the financial support from Landesforschungsförderung Hamburg (project: Health-Monitoring von Faserverbundstrukturen mit Hilfe von Sensorarrays, Grant No. LFF-FV 05). We thank OCSiAl, Russia for the support of the SWCNTs.

## References

[1] A. Parvizi, J.E. Bailey, On multiple transverse cracking in glass fibre epoxy cross-ply laminates, J. Mater. Sci. 13 (10) (1978) 2131–2136.
[2] A. Hosoi, S. Sakuma, Y. Fujita, H. Kawada, Prediction of initiation of transverse cracks in cross-ply CFRP laminates under fatigue loading by fatigue properties of unidirectional CFRP in 90° direction, Compos. Part A: Appl. Sci. Manuf. 68 (Complete) (2015) 398–405.
[3] D. Hull, Matrix-dominated properties of polymer matrix composite materials, Mater. Sci. Eng.: A 184 (2) (1994) 173–183.
[4] A.A. Griffith, The phenomena of rupture and flow in solids, Philos. Trans. Roy. Soc. Lond. A: Math. Phys. Eng. Sci. 221 (582–593) (1921) 163–198.
[5] P. Rose, Hochfeste c-fasern auf pan-basis, einsatzformen und eigenschaften im cfk-verbund, in: Verarbeiten und Anwenden kohlenstoffaserverstärkter Kunststoffe, VDI-Verlag, Düsseldorf, 1981, pp. 5–39.
[6] D.J. Thorne, Carbon fibres with large breaking strain, Nature 248 (5451) (1974) 754–756.
[7] A. Towse, K. Potter, M.R. Wisnom, R.D. Adams, Specimen size effects in the tensile failure strain of an epoxy adhesive, J. Mater. Sci. 33 (17) (1998) 4307–4314.
[8] T. Hobbiebrunken, B. Fiedler, M. Hojo, M. Tanaka, Experimental determination of the true epoxy resin strength using micro-scaled specimens, Compos. Part A: Appl. Sci. Manuf. 38 (3) (2007) 814–818.
[9] C. Leopold, W.V. Liebig, H. Wittich, B. Fiedler, Size effect of graphene nanoparticle modified epoxy matrix, Compos. Sci. Technol. 134 (2016) 217–225.
[10] R. Schueler, J. Petermann, K. Schulte, H.-P. Wentzel, Agglomeration and electrical percolation behavior of carbon black dispersed in epoxy resin, J. Appl. Polym. Sci. 63 (13) (1997) 1741–1746.
[11] D. Zhang, L. Ye, S. Deng, J. Zhang, Y. Tang, Y. Chen, CF/EP composite laminates with carbon black and copper chloride for improved electrical conductivity and interlaminar fracture toughness, Compos. Sci. Technol. 72 (3) (2012) 412–420.
[12] F.H. Gojny, M.H. Wichmann, B. Fiedler, K. Schulte, Influence of different carbon nanotubes on the mechanical properties of epoxy matrix composites – a comparative study, Compos. Sci. Technol. 65 (15–16) (2005) 2300–2313.
[13] M.H. Wichmann, J. Sumfleth, F.H. Gojny, M. Quaresimin, B. Fiedler, K. Schulte, Glass-fibre-reinforced composites with enhanced mechanical and electrical properties – benefits and limitations of a nanoparticle modified matrix, Eng. Fract. Mech. 73 (16) (2006) 2346–2359.
[14] S. Iijima, Helical microtubules of graphitic carbon, Nature 354 (6348) (1991) 56–58.
[15] S. Iijima, T. Ichihashi, Single-shell carbon nanotubes of 1-nm diameter, Nature 363 (6430) (1993) 603–605.
[16] M. Quaresimin, K. Schulte, M. Zappalorto, S. Chandrasekaran, Toughening mechanisms in polymer nanocomposites: from experiments to modelling, Compos. Sci. Technol. 123 (2016) 187–204.
[17] D.C. Davis, J.W. Wilkerson, J. Zhu, D.O. Ayewah, Improvements in mechanical properties of a carbon fiber epoxy composite using nanotube science and technology, Compos. Struct. 92 (11) (2010) 2653–2662.
[18] F.H. Gojny, M.H. Wichmann, U. Köpke, B. Fiedler, K. Schulte, Carbon nanotube-reinforced epoxy-composites: enhanced stiffness and fracture toughness at low nanotube content, Compos. Sci. Technol. 64 (15) (2004) 2363–2371.
[19] T.-H. Hsieh, A.J. Kinloch, A.C. Taylor, I.A. Kinloch, The effect of carbon nanotubes on the fracture toughness and fatigue performance of a thermosetting epoxy polymer, J. Mater. Sci. 46 (23) (2011) 7525–7535.
[20] M. Shtein, R. Nadiv, N. Lachman, H. Daniel Wagner, O. Regev, Fracture behavior of nanotube–polymer composites: insights on surface roughness and failure mechanism, Compos. Sci. Technol. 87 (2013) 157–163.
[21] F.H. Gojny, J. Nastalczyk, Z. Roslaniec, K. Schulte, Surface modified multi-walled carbon nanotubes in CNT/epoxy-composites, Chem. Phys. Lett. 370 (5–6) (2003) 820–824.
[22] J.B. Bai, A. Allaoui, Effect of the length and the aggregate size of MWNTs on the improvement efficiency of the mechanical and electrical properties of nanocomposites – experimental investigation, Compos. Part A: Appl. Sci. Manuf. 34 (8) (2003) 689–694.
[23] K.S. Novoselov, A.K. Geim, S.V. Morozov, D. Jiang, Y. Zhang, S.V. Dubonos, I.V. Grigorieva, A.A. Firsov, Electric field effect in atomically thin carbon films, Science 306 (5696) (2004) 666.
[24] A.K. Geim, K.S. Novoselov, The rise of graphene, Nat. Mater. 6 (3) (2007) 183–191.
[25] S. Chandrasekaran, N. Sato, F. Tölle, R. Mülhaupt, B. Fiedler, K. Schulte, Fracture toughness and failure mechanism of graphene based epoxy composites, Compos. Sci. Technol. 97 (2014) 90–99.
[26] L.-C. Tang, Y.-J. Wan, D. Yan, Y.-B. Pei, L. Zhao, Y.-B. Li, L.-B. Wu, J.-X. Jiang, G.-Q. Lai, The effect of graphene dispersion on the mechanical properties of graphene/epoxy composites, Carbon 60 (2013) 16–27.
[27] B. Ahmadi-Moghadam, M. Sharafimasooleh, S. Shadlou, F. Taheri, Effect of functionalization of graphene nanoplatelets on the mechanical response of graphene/epoxy composites, Mater. Des. (1980–2015) 66 (Part A) (2015) 142–149.
[28] M.A. Rafiee, J. Rafiee, Z. Wang, H. Song, Z.-Z. Yu, N. Koratkar, Enhanced mechanical properties of nanocomposites at low graphene content, ACS Nano 3 (12) (2009) 3884–3890.
[29] M.A. Rafiee, J. Rafiee, I. Srivastava, Z. Wang, H. Song, Z.-Z. Yu, N. Koratkar, Fracture and fatigue in graphene nanocomposites, Small 6 (2) (2010) 179–183.
[30] D.R. Bortz, E.G. Heras, I. Martin-Gullon, Impressive fatigue life and fracture toughness improvements in graphene oxide/epoxy composites, Macromolecules 45 (1) (2011) 238–245.
[31] M.-Y. Shen, T.-Y. Chang, T.-H. Hsieh, Y.-L. Li, C.-L. Chiang, H. Yang, M.-C. Yip, Mechanical properties and tensile fatigue of graphene nanoplatelets reinforced polymer nanocomposites, J. Nanomater. 2013 (4) (2013) 1–9.
[32] J.B. Knoll, B.T. Riecken, N. Kosmann, S. Chandrasekaran, K. Schulte, B. Fiedler, The effect of carbon nanoparticles on the fatigue performance of carbon fibre reinforced epoxy, Compos. Part A: Appl. Sci. Manuf. 67 (0) (2014) 233–240.
[33] I. Greenfeld, H.D. Wagner, Nanocomposite toughness, strength and stiffness: role of filler geometry, Nanocomposites 1 (1) (2015) 3–17.
[34] H. Liu, L.C. Brinson, Reinforcing efficiency of nanoparticles: a simple comparison for polymer nanocomposites, Compos. Sci. Technol. 68 (6) (2008) 1502–1512.
[35] B.T. Marouf, Y.-W. Mai, R. Bagheri, R.A. Pearson, Toughening of epoxy nanocomposites: nano and hybrid effects, Polym. Rev. 56 (1) (2016) 70–112.
[36] K. Diamanti, C. Soutis, Structural health monitoring techniques for aircraft composite structures, Prog. Aerosp. Sci. 46 (8) (2010) 342–352.
[37] M. Majumder, T.K. Gangopadhyay, A.K. Chakraborty, K. Dasgupta, D.K. Bhattacharya, Fibre Bragg gratings in structural health monitoring—present status and applications, Sens. Actuat. A: Phys. 147 (1) (2008) 150–164.
[38] S.S. Kessler, S.M. Spearing, C. Soutis, Damage detection in composite materials using lamb wave methods, Smart Mater. Struct. 11 (2) (2002) 269–278.
[39] J. Cai, L. Qiu, S. Yuan, L. Shi, P. Liu, D. Liang, Structural health monitoring for composite materials, in: N. Hu (Ed.), Composites and Their Applications, InTech, Rijeka, Croatia, 2012.
[40] W.J. Staszewski, C. Boller, G.R. Tomlinson, Health Monitoring of Aerospace Structures, John Wiley & Sons, Ltd, Chichester, UK, 2003.
[41] I. Kang, M.J. Schulz, J.H. Kim, V. Shanov, D. Shi, A carbon nanotube strain sensor for structural health monitoring, Smart Mater. Struct. 15 (3) (2006) 737–748.
[42] D.D.L. Chung, Structural health monitoring by electrical resistance measurement, Smart Mater. Struct. 10 (4) (2001) 624–636.
[43] K. Schulte, C. Baron, Load and failure analyses of CFRP laminates by means of electrical resistivity measurements, Compos. Sci. Technol. 36 (1) (1989) 63–76.
[44] J. Abry, In situ detection of damage in CFRP laminates by electrical resistance measurements, Compos. Sci. Technol. 59 (6) (1999) 925–935.

[45] J. Wen, Z. Xia, F. Choy, Damage detection of carbon fiber reinforced polymer composites via electrical resistance measurement, Compos. Part B: Eng. 42 (1) (2011) 77–86.
[46] A. Kaddour, F. Al-Salehi, S. Al-Hassani, M. Hinton, Electrical resistance measurement technique for detecting failure in CFRP materials at high strain rates, Compos. Sci. Technol. 51 (3) (1994) 377–385.
[47] R. Schueler, S.P. Joshi, K. Schulte, Damage detection in CFRP by electrical conductivity mapping, Compos. Sci. Technol. 61 (6) (2001) 921–930.
[48] M. Kupke, K. Schulte, R. Schüler, Non-destructive testing of FRP by d.c. and a.c. electrical methods, Compos. Sci. Technol. 61 (6) (2001) 837–847.
[49] K. Takahashi, H.T. Hahn, Towards practical application of electrical resistance change measurement for damage monitoring using an addressable conducting network, Struct. Health Monit. 11 (3) (2012) 367–377.
[50] H.D. Roh, H. Lee, Y.-B. Park, Structural health monitoring of carbon-material-reinforced polymers using electrical resistance measurement, Int. J. Prec. Eng. Manuf.-Green Technol. 3 (3) (2016) 311–321.
[51] N. Muto, Y. Arai, S. Shin, H. Matsubara, H. Yanagida, M. Sugita, T. Nakatsuji, Hybrid composites with self-diagnosing function for preventing fatal fracture, Compos. Sci. Technol. 61 (6) (2001) 875–883.
[52] B. Fiedler, F.H. Gojny, M.H.G. Wichmann, W. Bauhofer, K. Schulte, Can carbon nanotubes be used to sense damage in composites?, Ann Chim. Sci. Matér. 29 (6) (2004) 81–94.
[53] E.T. Thostenson, T.-W. Chou, Carbon nanotube networks: sensing of distributed strain and damage for life prediction and self healing, Adv. Mater. 18 (21) (2006) 2837–2841.
[54] M.H.G. Wichmann, S.T. Buschhorn, J. Gehrmann, K. Schulte, Piezoresistive response of epoxy composites with carbon nanoparticles under tensile load, Phys. Rev. B 80 (24) (2009).
[55] L. Böger, M.H. Wichmann, L.O. Meyer, K. Schulte, Load and health monitoring in glass fibre reinforced composites with an electrically conductive nanocomposite epoxy matrix, Compos. Sci. Technol. 68 (7–8) (2008) 1886–1894.
[56] C. Viets, S. Kaysser, K. Schulte, Damage mapping of GFRP via electrical resistance measurements using nanocomposite epoxy matrix systems, Compos. Part B: Eng. 65 (2014) 80–88.
[57] Alamusi, N. Hu, H. Fukunaga, S. Atobe, Y. Liu, J. Li, Piezoresistive strain sensors made from carbon nanotubes based polymer nanocomposites, Sensors (Basel, Switzerland) 11 (11) (2011) 10691–10723.
[58] H. Meeuw, C. Viets, W.V. Liebig, K. Schulte, B. Fiedler, Morphological influence of carbon nanofillers on the piezoresistive response of carbon nanoparticle/epoxy composites under mechanical load, Eur. Polym. J. 85 (2016) 198–210.
[59] F. Panozzo, M. Zappalorto, M. Quaresimin, Analytical model for the prediction of the piezoresistive behavior of CNT modified polymers, Compos. Part B: Eng. 109 (2017) 53–63.
[60] D. Stauffer, A. Aharony, Introduction to Percolation Theory, second ed., Taylor & Francis, London and Washington, DC, 1992.
[61] J.Z. Kovacs, B.S. Velagala, K. Schulte, W. Bauhofer, Two percolation thresholds in carbon nanotube epoxy composites, Compos. Sci. Technol. 67 (5) (2007) 922–928.
[62] W. Bauhofer, J.Z. Kovacs, A review and analysis of electrical percolation in carbon nanotube polymer composites, Compos. Sci. Technol. 69 (10) (2009) 1486–1498.
[63] R.A. Monetti, E.V. Albano, Critical behavior of the site percolation model on the square lattice in a LXM geometry - monte carlo and finite-size scaling study, Z. Phys. B - Condens. Matter (Z. Phys. B Condens. Matter) 82 (1) (1991) 129–134.
[64] S.J. Marrink, M.A. Knackstedt, Finite size scaling for percolation on elongated lattices in two and three dimensions, Phys. Rev. E 62 (3) (2000) 3205–3214.
[65] Y. Tang, L. Ye, Z. Zhang, K. Friedrich, Interlaminar fracture toughness and CAI strength of fibre-reinforced composites with nanoparticles – a review, Compos. Sci. Technol. 86 (2013) 26–37.
[66] ASTM International, Test Method for Tensile Strength and Youngs Modulus for High-modulus Single-filament Materials (Withdrawn 1998), 1975.
[67] K. Arakawa, K. Takahashi, Relationships between fracture parameters and fracture surface roughness of brittle polymers, Int. J. Fract. 48 (2) (1991) 103–114.
[68] D. Haba, A.J. Brunner, G. Pinter, Dispersion of fullerene-like WS2 nanoparticles within epoxy and the resulting fracture mechanics, Compos. Sci. Technol. 119 (2015) 55–61.
[69] J. Sandler, J.E. Kirk, I.A. Kinloch, M. Shaffer, A.H. Windle, Ultra-low electrical percolation threshold in carbon-nanotube-epoxy composites, Polymer 44 (19) (2003) 5893–5899.
[70] Y. Yu, G. Song, L. Sun, Determinant role of tunneling resistance in electrical conductivity of polymer composites reinforced by well dispersed carbon nanotubes, J. Appl. Phys. 108 (8) (2010) 084319.
[71] X. Shui, D.D.L. Chung, A piezoresistive carbon filament polymer-matrix composite strain sensor, Smart Mater. Struct. 5 (2) (1996) 243–246.